A novel method for automated assessment of megakaryocyte differentiation and proplatelet formation

Salzmann, Manuel; Hoesel, B.; Haase, M.; Mussbacher, M.; Schrottmaier, WC.; Kral-Pointner, JB.; Finsterbusch, M.; Mazharian, Alexandra; Assinger, Alice; Schmid, Johannes A.

DOI:
10.1080/09537104.2018.1430359

Platelets

ISSN: 0953-7104 (Print) 1369-1635 (Online) Journal homepage: http://www.tandfonline.com/loi/iplt20

A novel method for automated assessment of megakaryocyte differentiation and proplatelet formation

M. Salzmann, B. Hoesel, M. Haase, M. Mussbacher, WC. Schrottmaier, JB. Kral-Pointner, M. Finsterbusch, A. Mazharian, A. Assinger & JA. Schmid

To cite this article: M. Salzmann, B. Hoesel, M. Haase, M. Mussbacher, WC. Schrottmaier, JB. Kral-Pointner, M. Finsterbusch, A. Mazharian, A. Assinger & JA. Schmid (2018): A novel method for automated assessment of megakaryocyte differentiation and proplatelet formation, Platelets, DOI: 10.1080/09537104.2018.1430359

To link to this article: https://doi.org/10.1080/09537104.2018.1430359

http://www.tandfonline.com/iplt
ISSN: 0953-7104 (print), 1369-1635 (electronic)

platelets

Platelets, Early Online: 1–8
Published with license by Taylor & Francis. DOI: https://doi.org/10.1080/09537104.2018.1430359

Taylor & Francis
Taylor & Francis Group

METHOD ARTICLE

A novel method for automated assessment of megakaryocyte differentiation and proplatelet formation

M. Salzmann [1], B. Hoesel[1], M. Haase[1], M. Mussbacher[1], WC. Schrottmaier[1], JB. Kral-Pointner[1], M. Finsterbusch [1], A. Mazharian [2], A. Assinger[1], & JA. Schmid [1]

[1]*Institute of Vascular Biology and Thrombosis Research, Medical University of Vienna, Vienna, Austria and* [2]*Institute of Cardiovascular Sciences, College of Medical and Dental Sciences, University of Birmingham, Birmingham, UK*

Abstract

Transfusion of platelet concentrates represents an important treatment for various bleeding complications. However, the short half-life and frequent contaminations with bacteria restrict the availability of platelet concentrates and raise a clear demand for platelets generated *ex vivo*. Therefore, *in vitro* platelet generation from megakaryocytes represents an important research topic. A vital step for this process represents accurate analysis of thrombopoiesis and proplatelet formation, which is usually conducted manually. We aimed to develop a novel method for automated classification and analysis of proplatelet-forming megakaryocytes *in vitro*. After fluorescent labelling of surface and nucleus, MKs were automatically categorized and analysed with a novel pipeline of the open source software *CellProfiler*. Our new workflow is able to detect and quantify four subtypes of megakaryocytes undergoing thrombopoiesis: proplatelet-forming, spreading, pseudopodia-forming and terminally differentiated, anucleated megakaryocytes. Furthermore, we were able to characterize the inhibitory effect of dasatinib on thrombopoiesis in more detail. Our new workflow enabled rapid, unbiased, quantitative and qualitative in-depth analysis of proplatelet formation based on morphological characteristics. Clinicians and basic researchers alike will benefit from this novel technique that allows reliable and unbiased quantification of proplatelet formation. It thereby provides a valuable tool for the development of methods to generate platelets *ex vivo* and to detect effects of drugs on megakaryocyte differentiation.

Keywords

CellProfiler, computer-assisted image analysis, megakaryocytes, megakaryopoiesis, proplatelets, thrombopoiesis

History

Received 17 November 2017
Revised 4 January 2018
Accepted 4 January 2018
Published online 19 February 2018

Introduction

Nearly 7000 units of platelet concentrates are needed daily only in the United States (1). However, platelet concentrates have a limited shelf life of only 5 days and bacterial contaminations pose a serious risk of sepsis to recipients (2). Attempts to generate platelets *in vitro*, in order to circumvent these issues, have encountered major problems and only resulted in a limited number of functional platelets (3). Thus, successful generation of platelets *ex vivo* remains an unsolved, yet important aim (4–6). Essential steps to achieve this goal include uncovering of the molecular mechanisms controlling proplatelet formation and development of a method that allows a robust assessment of platelet formation from megakaryocytes (MKs) *in vitro*.

One of the most commonly assessed parameters of MK maturation is the percentage of proplatelet-forming MKs, which can vary from 10 to over 60% (7–21), depending on the specific quantification technique and the person that scores the MK phenotype. A first attempt to simplify and standardize the quantification of proplatelet formation used an *ImageJ* macro that distinguishes round from proplatelet-producing cells (22). This was a major step forward in improving analysis of proplatelet formation, but did not provide all the information needed to understand the processes of platelet generation in more detail.

Here, we developed a novel method, using the open source software *CellProfiler*, allowing an automated identification, quantification and in-depth characterization of four MK subsets during thrombopoiesis. Our computerized image analysis routine allows identification of undifferentiated, round MKs as well as proplatelet-forming MKs with long, thin extensions, spread MKs with a huge cellular area, pseudopodia-forming MKs with short, thick extensions and terminally differentiated MKs that lack a nucleus. Furthermore, additional information can be extracted, including intensities of biological markers and geometric parameters such as cell area, as a marker for MK spreading and consequently functionality (12,17–19,23). Based on available sources of stem cells and ethics allowances, we applied our novel image analysis to murine MKs cultured on fibrinogen as this extracellular matrix component of the vascular niche of the bone marrow has been

Correspondence: Johannes A. Schmid, Medical University of Vienna, Institute of Vascular Biology and Thrombosis Research, Schwarzspanierstraße 17 Vienna, 1090 Austria. Tel: 0043-1-40160-31155. E-mail: johannes.schmid@meduniwien.ac.at

Color versions of one or more of the figures in the article can be found online at www.tandfonline.com/iplt.

reported to foster proplatelet formation in mice (21). We are aware that human MKs differ from their murine counterparts given that antibodies blocking the fibrinogen receptor $\alpha_{IIb}\beta_3$ did not impede proplatelet development in human cells (12) and MKs from patients with a mutated, constitutive active fibrinogen receptor showed impaired proplatelet formation (24). Nevertheless, the image analysis technique that we developed for murine MKs has the potential to be applied to MKs from different species and on various matrices, as clearly distinct classes of morphological features are scored and quantified. While the biological relevance of the different categories that we observed is still not clear, we are confident that our method provides an improvement over the coarse differentiation of MKs into immature and proplatelet-forming cells.

Material and methods

MK purification and culture

Mature bone marrow-derived MKs were generated as previously described (20). Briefly, femora of mice were flushed and cells expressing Ly6G, CD11b, CD16/32 and B220 were depleted using magnetic beads (sheep anti-rat IgG Dynabeads, Invitrogen) and the following antibodies: anti-mouse Ly6G (eBioscience), anti-mouse CD11b (eBioscience), anti-mouse CD16/CD32 (BD Bioscience) and anti-mouse B220 (BD Bioscience), respectively. The remaining cells were incubated in Stempro-34 SFM (Invitrogen) with 2.6% nutrient supplement, 1% glutamine and 1% penicillin-streptomycin-fungizone (PSF) for 2 days in the presence of 20 ng/mL murine stem cell factor (SCF, Peprotech) followed by additional 5 days with 20 ng/mL SCF and 50 ng/mL murine thrombopoietin (TPO, Peprotech). At day 7, mature MKs were enriched using a 3%/1.5%/0% BSA (PAA Laboratories) gradient under gravity for 45 minutes at room temperature.

MK spreading and proplatelet formation assay

Spreading was performed as previously described (20). Slides were coated overnight with 100 µg/ml fibrinogen at room temperature and blocked for 1 hour with 1% BSA at 37°C. Untreated mature MKs or MKs treated with 10 µM dasatinib or DMSO were allowed to adhere and form proplatelets for 5 hours at 37°C, a time period that has been suggested by several reports (7,12,15,17–20). Fixed cells were permeabilized with 0.5% Triton X-100 and labelled with anti-mouse CD41-Alexa Fluor 488 (BioLegend), anti-alpha tubulin-eFluor615 (eBioscience), phalloidin-Alexa Fluor 555 (Molecular Probes) and 5 µg/mL Hoechst 33342 (Molecular Probes). Images were taken with a Nikon A1 plus confocal laser-scanning microscope, using a Plan Apo λ 10x objective (Nikon) NA: 0.45, a Plan Apo λ 20x objective (Nikon) NA: 0.75 and an Apo 40x WI λS DIC N2 objective (Nikon) NA: 1.25. Imaging Software: Nikon NIS-Elements Confocal 4.20.01.

Analysis of proplatelet formation

Images were analysed with the open source software *CellProfiler 3.0.0* (25) (http://cellprofiler.org/). The pipeline and detailed settings to reproduce the image analysis procedure are available at: http://cellprofiler.org/examples/published_pipelines. MKs were categorized into the following subtypes: proplatelet-forming MKs (Form Factor ≤ 0.19), spreading MKs (Form Factor > 0.19, Area > 6000 µm^2), pseudopodia-forming MKs (Form Factor > 0.19, Area ≤ 6000 µm^2, Compactness > 1.25), undifferentiated MKs (Form Factor > 0.19, Area ≤ 6000 µm^2, Compactness ≤ 1.25). "Form Factor" is described as $\frac{4\,\text{Area}}{Perimeter^2}$ (26), meaning a perfect circle has a value of 1. "Compactness" is the variance of the distance of the cells' pixels from the centroid divided by the area (26). A perfect circle, having no variances in pixel-centroid distances, has therefore a Compactness value of 0. Manual counting was conducted by searching for MKs with long, thin extensions.

Statistical analysis

Calculations were performed using GraphPad Prism 6.01 software. Data were analysed using Student's t-test or two-way ANOVA and Sidak's multiple comparison test. Statistical significances are depicted as: * $p \leq 0.05$, ** $p \leq 0.01$, *** $p \leq 0.001$, **** $p \leq 0.0001$. Bars are mean; error bars represent standard deviation (SD).

Results and discussion

Mature bone marrow-derived MKs were allowed to spread on fibrinogen – a method used to foster proplatelet formation, fixed and stained for CD41 and DNA followed by confocal imaging. While we were able to detect cells that showed typical proplatelet-forming shapes as known from literature (Figure 1A), other cells could not be categorized clearly (Figure 1B-D). This may explain the variation in the percentage of proplatelet-forming MKs found in different studies (7–21) (Supplemental Table 1). There have been previous attempts to classify maturing MKs into different stages, and proplatelet-forming MKs have been dissected into two developmental stages (7,27–29). Our morphological evaluation revealed five major subtypes, which can be described as follows:

(1) Proplatelet-forming MKs: cells with tubulin-positive extensions ≤ 10 µm thin and a length exceeding the cell body axis twofold or MKs with high protrusion complexity (Figure 1A).
(2) Spread MKs: large MKs that contain actin nodules (Figure 1B) as previously reported (18,30). Due to their large, flat cell bodies, they clearly differ from normal, round undifferentiated MKs, but cannot be considered classical proplatelet-forming MKs either.
(3) Pseudopodia-forming MKs: cells with tubulin positive cellular extensions that are too thick and/or short to be classified proplatelet-forming MKs (Figure 1C).
(4) Terminally differentiated MKs: anucleated MKs (Figure 1D) that could reflect the *in vivo* situation of nucleus extrusion and degradation at the final phase of thrombopoiesis (31).
(5) Undifferentiated MKs: Small round, nucleated cells (Figure 1E).

In order to objectively classify these distinct subsets, we measured morphological parameters of MKs that were representative for the different subclasses using the free image analyses software package *CellProfiler*. Thereby, we tried to describe the five categories mathematically in a most accurate, yet simple way. The resulting differentiation parameters such as form factor, area or compactness were used to establish an automated analysis routine (available at: http://cellprofiler.org/examples/published_pipelines). First, nucleated and anucleated MKs were identified from fluorescence images based on their CD41 and Hoechst 33342 staining (Figure 2Ai) and smoothed to prevent perimeter to area ratio artefacts (Figure 2Aii). Cells were then classified into five different subtypes and additional quantitative information like marker intensities, cell area or the number of adjacent cells can be extracted (Figure 2Aiii).

Terminally differentiated MKs that lack a nucleus (Figure 1D) were identified in the first step of CellProfiler analysis and did not need further classification (Figure 2). The second step classified nucleated MKs following a series of morphological and

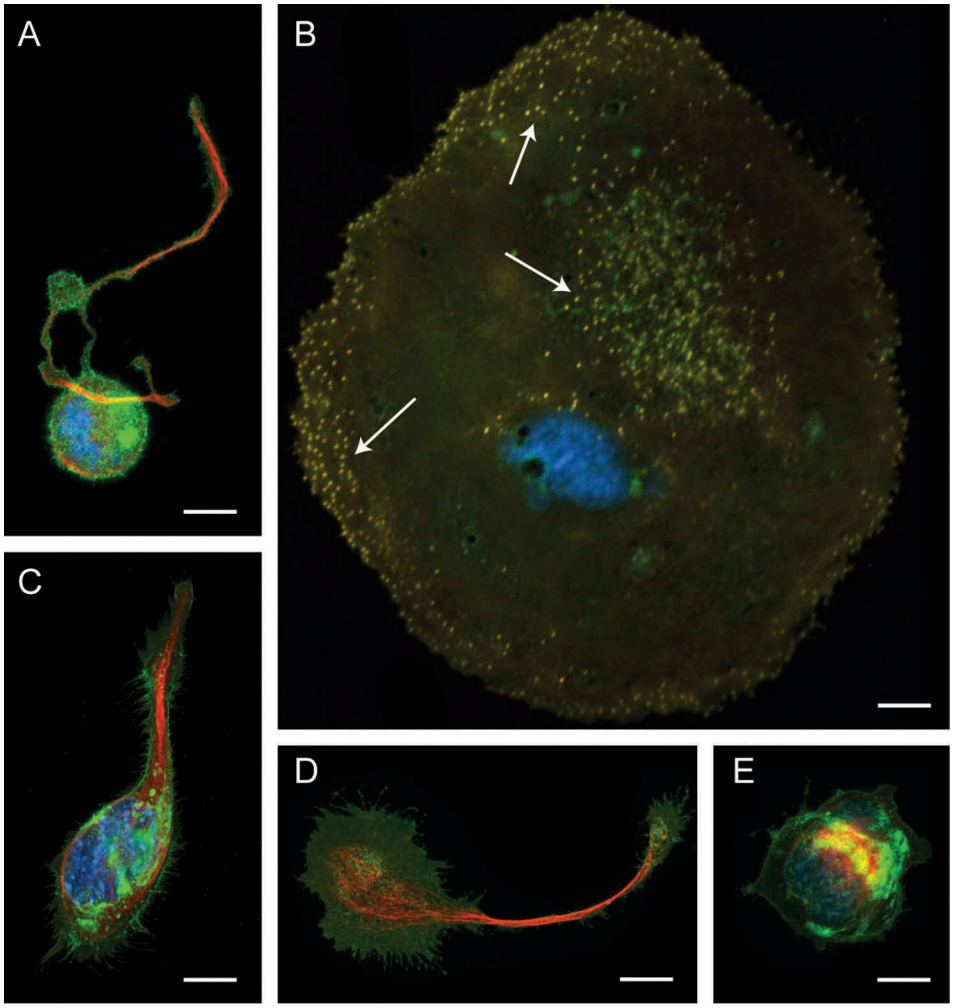

Figure 1. Five distinct morphological subtypes of MKs were observed, when performing a proplatelet formation assay. Mature MKs derived from murine femoral bone marrow were incubated for 5 hours on 100 µg/ml fibrinogen at 37°C, fixed and labelled with a MK specific anti-mouse CD41-Alexa Fluor 488 antibody (green), anti-alpha tubulin-eFluor615 antibody (red) or phalloidin-Alexa Fluor 555 (yellow) and counterstained with 5 µg/mL Hoechst 33342 to stain DNA (blue). (A) Proplatelet-forming MKs with long, thin, tubulin-positive extensions. (B) Spread MKs with actin nodules, indicated by white arrows, have a large cell area. (C) Pseudopodia-forming MKs with tubulin-positive extensions, which are thicker and/or shorter than proplatelet-forming cells. (D) Terminally differentiated MKs in the final phase of differentiation lack a nucleus. (E) Undifferentiated MKs as defined by their small and round shape. Arrangement of 5 individual images. Scale bar: 20 µm.

geometrical criteria, depicted in Figure 2B. Threshold values were selected empirically based on *CellProfiler* analysis of manually classified cells (meeting the above-mentioned criteria), using representative images.

The second subtype to be identified are morphologically complex proplatelet-forming MKs (Figure 1A), described by a Form Factor ≤ 0.19. Cells with a simpler morphology were further classified depending on their size. Cells with an area $>$ 6000 µm^2 were considered spread MKs (Figure 1B). Applying the selection criteria for spread MKs as a second step ensures that MKs with long, complex proplatelets that may exceed 6000 µm^2 cell area are correctly classified as proplatelet-forming MKs. Finally, pseudopodia-forming MKs (Figure 1C) were distinguished from round, undifferentiated MKs (Figure 1E) using a Compactness threshold of 1.25. This pseudopodia-forming cells might represent early stages of proplatelet formation; a hypothesis, which may be tested in future studies involving time-lapse microscopy of MK maturation.

To validate our pipeline, we compared manually and automatically analysed images (Figure 3A). The results show a significant inter-observer variability. This was apparently due to interpretation disparity between proplatelet-forming MKs and what we now define as pseudopodia-forming MKs having thicker extensions. The comparison between manual and computer-based evaluation of proplatelet-forming cells indicated that some individuals tend to score MKs with pseudopodia as proplatelet-forming. These inter-observer differences might also explain at least in part the huge variation of the reported percentages of proplatelet-forming MKs in literature, which might also depend on matrix type, cell source and MK incubation time (Supplemental Table 1). The computer-based method was clearly more stringent and could furthermore analyse substantially more cells without additional effort, leading to a more accurate result (Figure 3A). To test whether the complex morphology of MKs impedes *CellProfiler*'s automated cell identification, we also compared the automated cell recognition and separation with a manual segregation of cells by drawing a background-coloured line between overlapping or touching cells (Figure 3B). In total, 3788 automatically separated and 3805 manually separated cells were identified and analysed, without observing significant differences in percentages (Figure 3C, 3D) or cell areas (Figure 3E) of all differentiated MKs combined. Noteworthy, the mean percentages of differentiated, i.e. usually defined as proplatelet-forming MKs as

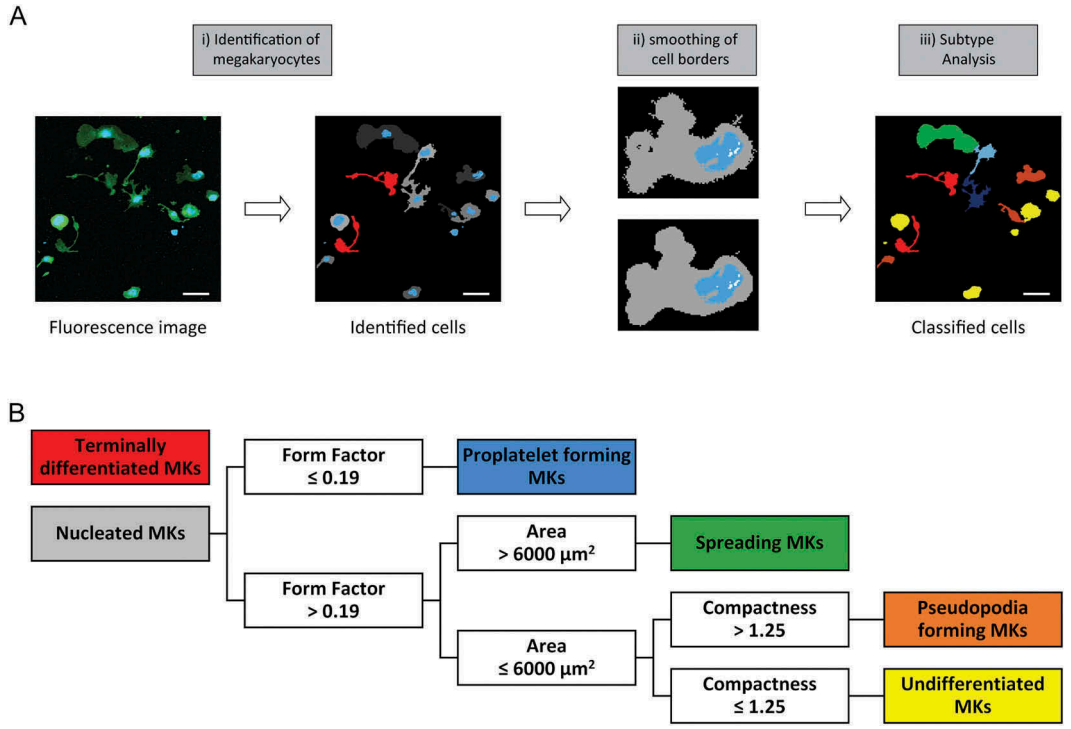

Figure 2. Workflow of automated MK analysis. (A) Fluorescence images with CD41 as MK marker and Hoechst 33342 as nuclear stain were processed with CellProfiler to identify nucleated and anucleated cells (i). To prevent perimeter to area ratio artefacts, images of cell borders were smoothed (ii). Smoothed cells were analysed with CellProfiler and classified into five distinct subsets, according to their morphology (iii). (B) The workflow to classify the subsets works as follows: Nucleated and anucleated (terminally differentiated) MKs were first identified based on the presence of a nucleus. With our self-designed CellProfiler pipeline, nucleated MKs are then classified based on their Form Factor (complexity of shape), cell area and Compactness (roundness). The MK subsets are proplatelet-forming (blue), spreading (green), pseudopodia forming (orange), terminally differentiated (red) and undifferentiated (yellow) MKs. Scale bar: 100 µm.

described in literature (7–21) is in line with the sum of all differentiated MK-categories of our analysis (22.87 ± 16.03% vs 32.86 ± 2.73%, respectively; Figure 3C). However, a more detailed discrimination, using our computer-based analysis tool, revealed that only part of differentiated MKs scored as proplatelet-forming, with a much higher percentage of cells exhibiting pseudopodia (Figure 3D).

This showed that our algorithm accurately identifies the complex morphology of MKs and is able to segregate overlapping or touching cells with its automated separation routine.

Using this automated and unbiased analysis, we observed 3.9% proplatelet-forming, 6.1% spreading, 17.8% pseudopodia-forming and 5.6% terminally differentiated MKs under our culture conditions (Figure 3D). Pseudopodia-forming MKs with an average of 3054 µm^2 had twofold less cell area than MKs forming actual proplatelets (Figure 3F), demonstrating that although they resemble proplatelet-forming MKs at first glance, they significantly differ in their cell area due to their lack of proper proplatelets. These may represent cells that are just initiating proplatelet formation. Seeding cells at varying densities did not result in significant differences in the total numbers of differentiated cells. However, a slight reduction of pseudopodia-forming MKs was observed at lower cell densities. (Supplemental Figure 1).

To further evaluate the applicability of our automated MK classification for pharmacological studies we treated cells with dasatinib, a drug that is known to influence MK maturation and to cause mild thrombocytopenia in patients. It is a potent, ATP-competitive inhibitor of several tyrosine kinases, which diminishes proplatelet formation and spreading *in vitro* (17). Applying our automated workflow, we observed almost exactly the same significant overall decrease in MKs undergoing thrombopoiesis as previously reported: The percentage of differentiating MKs decreased in presence of dasatinib from 32.3 to 13.9% (Figure 4A), whereas spread MKs and pseudopodia-forming MKs were affected the most (8.4 to 0.6% and 17.0 to 8.7%, respectively). Proplatelet-forming MKs also decreased from 1.7 to 0.2% (Figure 4B) and could only be detected in one sample. Furthermore, dasatinib also decreased the mean cell area from 2620 µm^2 to 1148 µm^2 (Figure 4C), with proplatelet-forming MKs being reduced by 71% from 8170 µm^2 to 2375 µm^2 (Figure 4D). Representative images of MKs treated with dasatinib are shown in Figure 4E. Hence the reduction of MKs undergoing thrombopoiesis was mainly due to diminished proplatelet-forming and spreading MKs and a reduction of pseudopodia-forming MKs. Furthermore, cell area of proplatelet-forming MKs was decreased upon dasatinib treatment, also confirming a reduction of proplatelets. These observations on the inhibitory effect of dasatinib on thrombopoiesis provide a deeper insight into the cause of mild thrombocytopenia that is noticed in patients treated with dasatinib for imatinib-resistant chronic myelogenous leukaemia (17). In order to test our image analysis routine and the effect of dasatinib treatment on a different matrix than fibrinogen, we furthermore performed experiments with MKs seeded on fibronectin. There we found a similar reduction in proplatelet and pseudopodia formation, however, with higher variability and a higher fraction of anucleated MKs (Supplemental Figure 2).

Conclusion

We provide a novel, automated, reproducible and sensitive method to evaluate differentiation and proplatelet formation of MKs based on their morphology. Besides introducing new MK

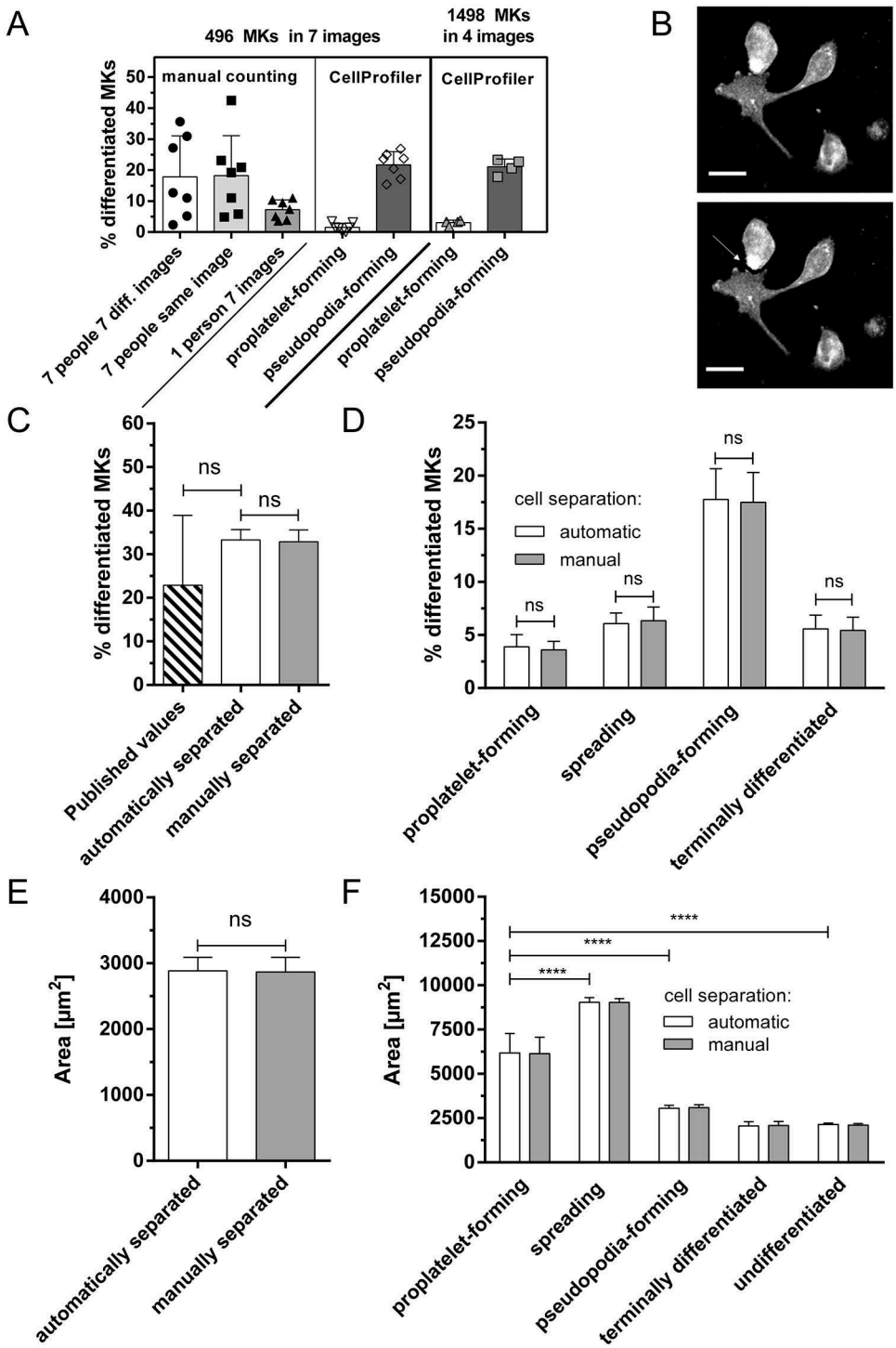

Figure 3. Mature MKs were incubated for 5 hours on fibrinogen at 37°C to allow proplatelet formation. Cells were then fixed and stained with CD41 as MK marker and Hoechst 33342. (A) Seven individuals identified proplatelet-forming MKs based on long, thin extensions on seven different images (about 70 cells/image). Additionally, one image was analysed by all people and one person counted proplatelet-forming MKs on all images. Results were compared with our automated Cellprofiler pipeline. (B) Prior to analysis with our pipeline, images were duplicated and cells on one duplicate manually separated to ease automated cell recognition. A line in background colour was drawn between adjacent cells to separate them clearly. The white arrow indicates the line that was drawn. (C) Percentages of proplatelet-forming MKs found in literature (see Suppl. Tab. 1) and of differentiated MKs with automatic and manual separation of cells. (D) Percentages of proplatelet-forming MKs, spreading MKs, pseudopodia forming MKs, terminally differentiated and undifferentiated MKs. (E) Cell area of differentiated MKs of automatically separated and manually separated cells. (F) Cell area of proplatelet-forming MKs, spreading MKs, pseudopodia forming MKs, terminally differentiated and undifferentiated MKs. Mean ± SD of 3 biological replicates, with an average cell number of 3902–3765 automatically and manually separated MKs, respectively. Scale bar: 50 µm.

subtypes during thrombopoiesis, our method provides solid comparability with previous reports, as the results of our automated MK cell classification are in line with published values of manually counted cells, while being more time-effective and unbiased. Variations between studies may partially derive from non-standardized definition of proplatelet-forming MKs and from individual differences in morphology assessments. Our novel workflow is sensitive enough to monitor and quantify not only reported changes in proplatelet formation but also spreading of MKs.

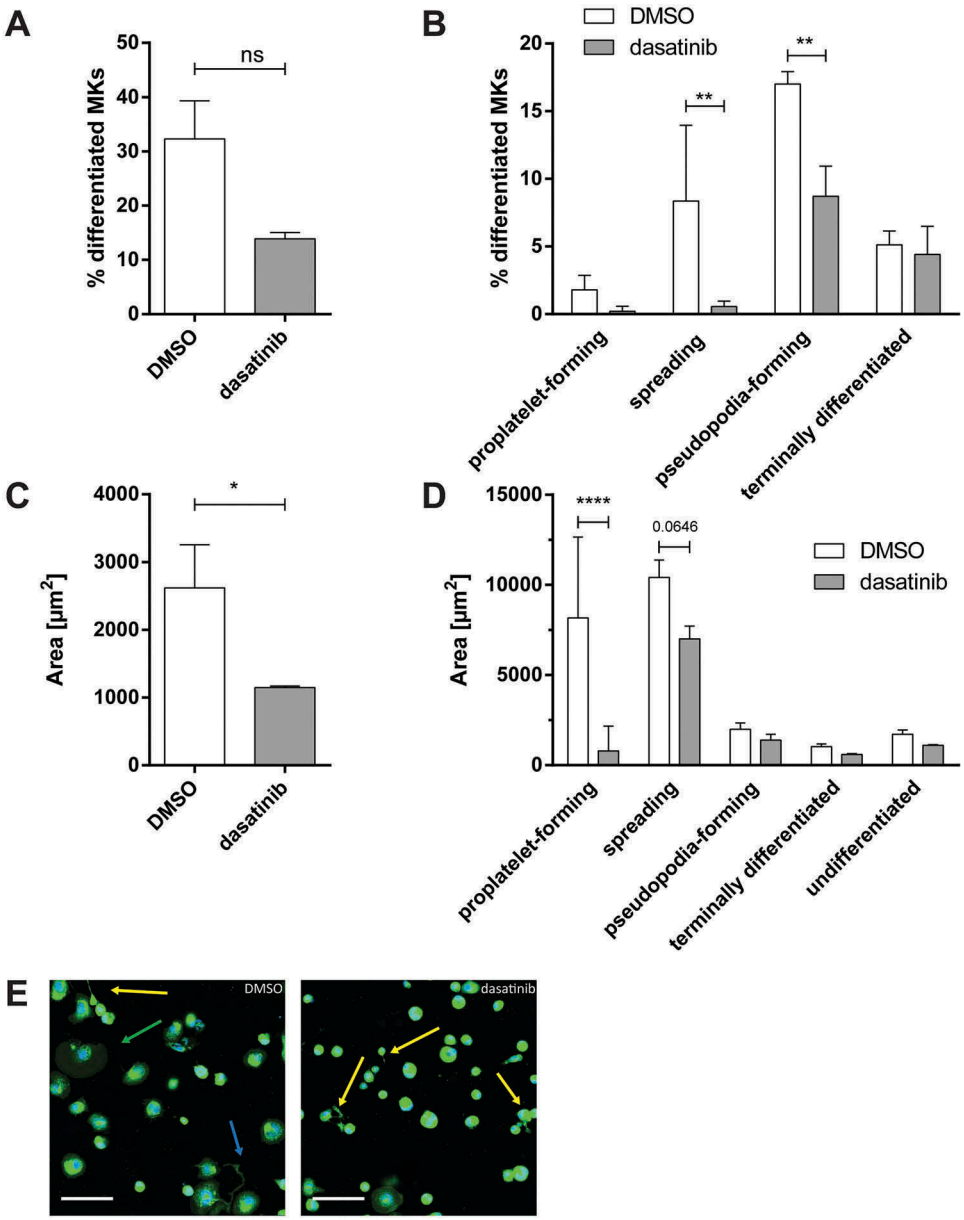

Figure 4. Mature MKs were treated with DMSO or 10 µM dasatinib for 15 min and incubated for 5 hours on fibrinogen at 37°C to allow proplatelet-formation. (A) Percentages of differentiated MKs after dasatinib or DMSO-control treatment. (B) Percentages of proplatelet-forming MKs, spreading MKs, pseudopodia-forming MKs, terminally differentiated and undifferentiated MKs. (C) Cell area of differentiated MKs of dasatinib-treated and DMSO-control cells. (D) Cell area of proplatelet-forming MKs, spreading MKs, pseudopodia forming MKs, terminally differentiated and undifferentiated MKs. (E) Representative, CD41-labelled image of DMSO treated and dasatinib-treated MKs. Blue arrow: proplatelet-forming MK; green arrow: spread MK; yellow arrows: pseudopodia-forming MKs. Mean ± SD of 3 biological replicates, with an average cell number of 570–855 DMSO and dasatinib treated MKs, respectively. Scale Bar: 150 µm.

The five categories of MK morphology that we distinguish with our approach might not directly reflect biological stages of the differentiation and maturation process. Furthermore, the transition from one category to another might be gradual. Future studies will be necessary to assign the expression of relevant marker or driver genes of MK maturation to the various categories that we propose here. Moreover, machine-learning methods of image analysis in combination with staining of relevant biomarkers might be applied for a more fine-tuned classification. This may result in even more categories and link the morphological categorization to a defined biological staging of MK maturation and proplatelet formation.

Although we used murine MKs derived from bone marrow stem cells, this pipeline is likely to be also applicable for MKs derived from other sources. In our standardized routine, we used fibrinogen, which is localized to vascular sinusoids (21) and represents a sound inducer of murine proplatelet formation *in vitro* (12,32). However, other methods to induce proplatelets would be equally possible and compatible with our CellProfiler's analysis, as long as fluorescent images of cell bodies and nuclei are analysed. The exact biological function of pseudopodia-forming MKs and spread MKs remains to be elucidated. However, we were able to observe a moderate reduction of pseudopodia-forming cells and a strong reduction of spread MKs after dasatinib treatment, indicating reduced MK function, leading to thrombocytopenia (17).

Taken together, we present a novel method for automated MK classification and quantification of proplatelet formation using a new pipeline for the free *CellProfiler* software. The advantage of our approach over current analysis tools is that it

reduces inter-institutional differences via introduction of an unbiased, investigator-independent and time-saving analysis tool, which can score a high number of cells in a robust and objective manner, thereby also improving statistical analyses. This opens the possibility for high-throughput screening of substances or treatments that influence MK maturation and development of proplatelets.

Yet, our method has the limitation that it relies on fluorescence staining of MKs and is thus not applicable to transmission light microscopy images of MKs. Furthermore, the analysis parameters that we worked out for our system (as defined in Figure 2) might have to be adjusted for the analysis of MKs from other sources or grown on other extracellular matrices. It is evident that computer-based image analysis cannot rule out miss-classification or erroneous cell segmentation completely; however, its automated, unbiased nature and the potential for classifying high numbers of cells outperforms manual, individual evaluation.

Overall, we are convinced that an improved quantification of platelet formation will provide a valuable basis for new insights in MK and platelet research, thereby fostering the development of *ex vivo* generation of platelets. Ultimately, this could reduce the demand of blood donors for platelet concentrates and would further offer the possibility for autologous platelet transfusion. As a consequence, recipient patients would benefit from diminished risks of infections or autoimmune diseases.

Acknowledgements

The authors wish to thank Hannah Paar, Susanne Humpeler and Sonja Bleichert for their excellent technical support and Bernhard Moser and Mario Kuttke for their help in manually counting proplatelet-forming MKs.

Furthermore, we are grateful for the financial support by the Austrian Science Fund FWF (project SFB-F54 to J.A. Schmid).

Conflict-of-interest disclosure

The authors report no declarations of interest.

Supplemental material

Supplemental data for this article can be access on the publisher's website

ORCID

M. Salzmann http://orcid.org/0000-0001-5477-3533
M. Finsterbusch http://orcid.org/0000-0001-9470-4313
A. Mazharian http://orcid.org/0000-0002-0204-3325
JA. Schmid http://orcid.org/0000-0002-6586-3507

References

1. American Red Cross. 2016. Blood Facts and Statistics. http://www.redcrossblood.org/learn-about-blood/blood-facts-and-statistics. [Accessed 2016 Nov 12].
2. Brecher ME, Hay SN. 2005. Bacterial contamination of blood components. Clin Microbiol Rev. 18(1):195–204. doi:10.1128/cmr.18.1.195-204.2005
3. Lambert MP, Sullivan SK, Fuentes R, French DL, Poncz M. 2013. Challenges and promises for the development of donor-independent platelet transfusions. Blood. 121(17):3319–3324. doi:10.1182/blood-2012-09-455428
4. Thon JN, Mazutis L, Wu S, Sylman JL, Ehrlicher A, Machlus KR, Feng Q, Lu S, Lanza R, Neeves KB et al. 2014. Platelet bioreactor-on-a-chip. Blood. 124(12):1857–1867.
5. Di Buduo CA, Wray LS, Tozzi L, Malara A, Chen Y, Ghezzi CE, Smoot D, Sfara C, Antonelli A, Spedden E et al. 2015. Programmable 3D silk bone marrow niche for platelet generation ex vivo and modeling of megakaryopoiesis pathologies. Blood. 125(14):2254–2264. doi:10.1182/blood-2014-08-595561
6. Di Buduo CA, Kaplan DL, Balduini A. 2017. In vitro generation of platelets: Where do we stand? Transfus Clin Biol. 24(3):273–276. doi:10.1016/j.tracli.2017.06.013
7. Aguilar A, Pertuy F, Eckly A, Strassel C, Collin D, Gachet C, Lanza F, Leon C. 2016. Importance of environmental stiffness for megakaryocyte differentiation and proplatelet formation. Blood. 128(16):2022–2032. doi:10.1182/blood-2016-02-699959
8. Bender M, Eckly A, Hartwig JH, Elvers M, Pleines I, Gupta S, Krohne G, Jeanclos E, Gohla A, Gurniak C et al. 2010. ADF/n-cofilin-dependent actin turnover determines platelet formation and sizing. Blood. 116(10):1767–1775. doi:10.1182/blood-2010-03-274340
9. Macaulay IC, Thon JN, Tijssen MR, Steele BM, MacDonald BT, Meade G, Burns P, Rendon A, Salunkhe V, Murphy RP et al. 2013. Canonical Wnt signaling in megakaryocytes regulates proplatelet formation. Blood. 121(1):188–196. doi:10.1182/blood-2012-03-416875
10. Bender M, Giannini S, Grozovsky R, Jonsson T, Christensen H, Pluthero FG, Ko A, Mullally A, Kahr WH, Hoffmeister KM et al. 2015. Dynamin 2-dependent endocytosis is required for normal megakaryocyte development in mice. Blood. 125(6):1014–1024. doi:10.1182/blood-2014-07-587857
11. Palazzo A, Bluteau O, Messaoudi K, Marangoni F, Chang Y, Souquere S, Pierron G, Lapierre V, Zheng Y, Vainchenker W et al. 2016. The cell division control protein 42 /Src family kinase/Neural Wiskott-Aldrich syndrome protein pathway regulates human proplatelet formation. J Thromb Haemost. doi:10.1111/jth.13519
12. Balduini A, Pallotta I, Malara A, Lova P, Pecci A, Viarengo G, Balduini CL, Torti M. 2008. Adhesive receptors, extracellular proteins and myosin IIA orchestrate proplatelet formation by human megakaryocytes. J Thromb Haemost. 6(11):1900–1907. doi:10.1111/j.1538-7836.2008.03132.x
13. Du C, Xu Y, Yang K, Chen S, Wang X, Wang S, Wang C, Shen M, Chen F, Chen M et al. 2017. Estrogen promotes megakaryocyte polyploidization via estrogen receptor beta-mediated transcription of GATA1. Leukemia. 31(4):945–956. doi:10.1038/leu.2016.285
14. Semeniak D, Kulawig R, Stegner D, Meyer I, Schwiebert S, Bosing H, Eckes B, Nieswandt B, Schulze H. 2016. Proplatelet formation is selectively inhibited by collagen type I through Syk-independent GPVI signaling. J Cell Sci. 129(18):3473–3484. doi:10.1242/jcs.187971
15. Hobbs CM, Manning H, Bennett C, Vasquez L, Severin S, Brain L, Mazharian A, Guerrero JA, Li J, Soranzo N et al. 2013. JAK2V617F leads to intrinsic changes in platelet formation and reactivity in a knock-in mouse model of essential thrombocythemia. Blood. 122(23):3787–3797. doi:10.1182/blood-2013-06-501452
16. Zhang L, Urtz N, Gaertner F, Legate KR, Petzold T, Lorenz M, Mazharian A, Watson SP, Massberg S. 2013. Sphingosine kinase 2 (Sphk2) regulates platelet biogenesis by providing intracellular sphingosine 1-phosphate (S1P). Blood. 122(5):791–802. doi:10.1182/blood-2012-12-473884
17. Mazharian A, Ghevaert C, Zhang L, Massberg S, Watson SP. 2011. Dasatinib enhances megakaryocyte differentiation but inhibits platelet formation. Blood. 117(19):5198–5206. doi:10.1182/blood-2010-12-326850
18. Mazharian A, Wang YJ, Mori J, Bem D, Finney B, Heising S, Gissen P, White JG, Berndt MC, Gardiner EE et al. 2012. Mice lacking the ITIM-containing receptor G6b-B exhibit macrothrombocytopenia and aberrant platelet function. Sci Signal. 5(248):ra78. doi:10.1126/scisignal.2002936
19. Mazharian A, Mori J, Wang YJ, Heising S, Neel BG, Watson SP, Senis YA. 2013. Megakaryocyte-specific deletion of the protein-tyrosine phosphatases Shp1 and Shp2 causes abnormal megakaryocyte development, platelet production, and function. Blood. 121(20):4205–4220. doi:10.1182/blood-2012-08-449272
20. Mazharian A, Watson SP, Severin S. 2009. Critical role for ERK1/2 in bone marrow and fetal liver-derived primary megakaryocyte differentiation, motility, and proplatelet formation. Exp Hematol. 37(10):1238–1249.e1235. doi:10.1016/j.exphem.2009.07.006

21. Larson MK, Watson SP. 2006. Regulation of proplatelet formation and platelet release by integrin alpha IIb beta3. Blood. 108(5):1509–1514. doi:10.1182/blood-2005-11-011957
22. Thon JN, Devine MT, Jurak Begonja A, Tibbitts J, Italiano JE, Jr. 2012. High-content live-cell imaging assay used to establish mechanism of trastuzumab emtansine (T-DM1)–mediated inhibition of platelet production. Blood. 120(10):1975–1984. doi:10.1182/blood-2012-04-420968
23. Mazharian A, Thomas SG, Dhanjal TS, Buckley CD, Watson SP. 2010. Critical role of Src-Syk-PLC{gamma}2 signaling in megakaryocyte migration and thrombopoiesis. Blood. 116(5):793–800. doi:10.1182/blood-2010-03-275990
24. Bury L, Malara A, Gresele P, Balduini A. 2012. Outside-In Signalling Generated by a Constitutively Activated Integrin αIIbβ3 Impairs Proplatelet Formation in Human Megakaryocytes. PLOS ONE. 7(4):e34449. doi:10.1371/journal.pone.0034449
25. Carpenter AE, Jones TR, Lamprecht MR, Clarke C, Kang IH, Friman O, Guertin DA, Chang JH, Lindquist RA, Moffat J et al. 2006. CellProfiler: image analysis software for identifying and quantifying cell phenotypes. Genome Biol. 7(10):R100. doi:10.1186/gb-2006-7-10-r100
26. 2018. Module: MeasureObjectSizeShape. [accessed 2016 23.Nov]. http://cellprofiler.org/manuals/current/MeasureObjectSizeShape.html
27. Strassel C, Eckly A, Leon C, Petitjean C, Freund M, Cazenave JP, Gachet C, Lanza F. 2009. Intrinsic impaired proplatelet formation and microtubule coil assembly of megakaryocytes in a mouse model of Bernard-Soulier syndrome. Haematologica. 94(6):800–810. doi:10.3324/haematol.2008.001032
28. Balduini A, Malara A, Balduini CL, Noris P. 2011. Megakaryocytes derived from patients with the classical form of Bernard-Soulier syndrome show no ability to extend proplatelets in vitro. Platelets. 22(4):308–311. doi:10.3109/09537104.2010.547960
29. Pouli D, Tozzi L, Alonzo CA, Liu Z, Kaplan DL, Balduini A, Georgakoudi I. 2017. Label free monitoring of megakaryocytic development and proplatelet formation in vitro. Biomed Opt Express. 8(10):4742–4755. doi:10.1364/boe.8.004742
30. Poulter NS, Pollitt AY, Davies A, Malinova D, Nash GB, Hannon MJ, Pikramenou Z, Rappoport JZ, Hartwig JH, Owen DM et al. 2015. Platelet actin nodules are podosome-like structures dependent on Wiskott-Aldrich syndrome protein and ARP2/3 complex. Nat Commun. 6:7254. doi:10.1038/ncomms8254
31. Machlus KR, Thon JN, Italiano JE, Jr. 2014. Interpreting the developmental dance of the megakaryocyte: a review of the cellular and molecular processes mediating platelet formation. Br J Haematol. 165(2):227–236. doi:10.1111/bjh.12758
32. Sim X, Poncz M, Gadue P, French DL. 2016. Understanding platelet generation from megakaryocytes: implications for in vitro-derived platelets. Blood. 127(10):1227–1233. doi:10.1182/blood-2015-08-607929